arXiv:1511.00745v3 [cond-mat.quant-gas] 3 Jun 2016

Properties of bosons in a one-dimensional bichromatic optical lattice in the regime of the Sine-Gordon transition: a Worm Algorithm Monte Carlo study

Asaad R. Sakhel[1,2]

[1]*Department of Physics and Basic Sciences, Faculty of Engineering Technology, Al-Balqa Applied University, Amman 11134, Jordan*

[2]*Abdus-Salam International Center for Theoretical Physics, Strada Costiera 11, 34151 Trieste, Italy*

(Dated: June 6, 2016)

The sensitivity of the Sine-Gordon (SG) transition of strongly interacting bosons confined in a shallow, one-dimensional (1D), periodic optical lattice (OL), is examined against perturbations of the OL. The SG transition has been recently realized experimentally by Haller *et al.* [Nature **466**, 597 (2010)] and is the exact opposite of the superfluid (SF) to Mott insulator (MI) transition in a deep OL with weakly interacting bosons. The continuous-space worm algorithm (WA) Monte Carlo method [Boninsegni *et al.*, Phys. Rev. E **74**, 036701 (2006)] is applied for the present examination. It is found that the WA is able to reproduce the SG transition which is another manifestation of the power of continuous-space WA methods in capturing the physics of phase transitions. In order to examine the sensitivity of the SG transition, it is tweaked by the addition of the secondary OL. The resulting bichromatic optical lattice (BCOL) is considered with a rational ratio of the constituting wavelengths λ_1 and λ_2 in contrast to the commonly used irrational ratio. For a weak BCOL, it is chiefly demonstrated that this transition is robust against the introduction of a weaker, secondary OL. The system is explored numerically by scanning its properties in a range of the Lieb-Liniger interaction parameter γ in the regime of the SG transition. It is argued that there should not be much difference in the results between those due to an irrational ratio λ_1/λ_2 and due to a rational approximation of the latter, bringing this in line with a recent statement by Boéris *et al.* [Phys. Rev. A **93**, 011601(R) (2016)]. The correlation function, Matsubara Green's function (MGF), and the single-particle density matrix do not respond to changes in the depth of the secondary OL V_1. For a stronger BCOL, however, a response is observed because of changes in V_1. In the regime where the bosons are fermionized, the MGF reveals that hole excitations are favored over particle excitatons manifesting that holes in the SG regime play an important role in the response of properties to changes in γ.

PACS numbers: 03.75.-b,03.75.Lm,67.85.-d,68.35.Rh,68.65.Cd,67.85.Hj

I. INTRODUCTION

It is known that weakly interacting bosons confined by a deep periodic one-dimensional (1D) optical lattice (OL) undergo a transition from a superfluid to a Mott insulator (MI) [1–4] when the strength of the OL is increased. The opposite situation of getting another kind of SF to MI transition in a shallow 1D OL occupied by strongly interacting bosons [5, 6] is known as the Sine-Gordon (SG) transition, where the bosons are "pinned" just by subjecting them to a very weak periodic OL. Indeed, the SG transition has been just recently realized experimentally [5], although its concept has been communicated and examined earlier [6, 7] even in a hollow-core 1D fibre [8]. In the phase diagram Fig.4 of Haller *et al.* [5], the SG regime exists for interactions $\gamma \geq \gamma_c = 3.5$ and a vanishingly shallow 1D OL of depth $V_0 < E_R$ where E_R is the recoil energy and γ (γ_c) the Lieb-Liniger (critical) interaction parameter [9].

The main goal of this article is the examination of the sensitivity of this pinning transition against perturbations. In that sense, we tweak the SG transition by the addition of a second disordering OL component; a method that has been used elsewhere [10–12]. Since the latter transition has been observed in a periodic OL [5], it is justified to explore its stability under a perturbation of the latter OL. In fact the chief result of this work is that the SG transition is robust against the latter perturbations. This result may turn out to be important in the research on hollow-core 1D fibres filled with ultracold atoms, where photons have been pinned by a shallow effective polaritonic potential just like atoms [8] and the quantum transport of strongly interacting photons [13].

Another goal is the examination of the properties of the bosons as measured by the pair correlation function $g_2(r)$ and one-body density matrix (OBDM) $g_1(r)$ (with r the distance between a pair of particles), the Matsubara Green's function (MGF) $G(p=0;\tau)$, and superfluid fraction ρ_s/ρ in the regime of this transition. Both of $g_2(r)$ and $g_1(r)$ are spatially averaged quantities as given below by Eqs.(9) and (15), respectively. It must be emphasized that in this work the $g_2(r)$ of the homogeneous Bose gas has been intentionally applied to the bosons in a 1D bichromatic optical lattice (BCOL), for mathematical convenience, to account for the density-density correlations under the effect of a BCOL. The pair correlations are inherently related to, and give an account of, the density-density correlations [14, 15]. On the other hand for inhomogeneous systems, the pair correlation function and OBDM are normalized by convolutions of the spatially varying density instead of the average linear density (a constant). These are given by what is equal to

$h_2(r) = g_2(r)n_0^2/\rho_c(r)$ and $h_1(r) = g_1(r)n_0/\rho_{c,\frac{1}{2}}(r)$ in Eqs.(14) and (16), respectively. Here $\rho_c(r)$ and $\rho_{c,\frac{1}{2}}(r)$ are defined by Eqs.(13) and (17), respectively, and n_0 is the average linear density. It is found that one can obain from $g_2(r)$ appreciable signals arising from a strong response to changes in the primary OL and interactions. Further, $g_1(r)$ applied to the BCOL system displays almost the same behavior as $h_1(r)$, except for some small differences. In $h_2(r)$, the normalization by $\rho_c(r)$ is found to weaken these signals substantially. A key result is that for a shallow 1D OL, the above properties are not influenced by perturbations of the OL, bringing this in line with a recent examination [16]. We particularly focus on $g_2(r)$ because it is important to examine it with regards to this and other kinds of phase transitions. For example the pair correlation function for a 1D uniform Bose gas has been used as the ratio between the photoassociation rates of Rb^{87} atoms in 1D and 3D [17]. Although we examine it only briefly, the $g_1(r)$ is also not any less important; for example Deissler *et al.* [18] presented the first experimental analysis of a spatially averaged $g_1(r)$, similar to ours, in a quasiperiodic optical lattice (QPOL).

Remaining within the regime of the SG–transition, we explore it in a BCOL instead of a 1D OL to study its sensitivity –in addition to that of the associated properties– to changes in the BCOL. Indeed the role of a 1D OL, such as the BCOL [10, 11], and in conjunction with atom-atom interactions in defining the properties of confined bosons lies at the heart of many investigations today [12, 17, 19–23]. So far, the BCOL has been mostly applied to introduce quasidisorder in a "common experimental route" [12]. This is usually achieved by superimposing two OL wavelengths whose ratio λ_1/λ_2 yields an irrational number [19, 21, 22]. However, the lattice setup with a rational number λ_1/λ_2 is not very common and deserves therefore an investigation, particularly due to the likelihood that there may be not much difference between the use of a rational and irrational λ_1/λ_2. The same argument has been made recently by Boeris *et al.* [16] who stated (quoting them): "... it is not necessary to implement truly irrational numbers with mathematical (i.e., unattainable) precision; after all, on a finite lattice one can "resolve" only a finite number of digits." In fact, real disorder can only be achieved by a speckle potential and the investigation of bosons in this kind of potential, and add to this a quasidisordered one, has been going on intensively in the last few years [11, 18, 20, 22, 24–52]. The minor side issue on the difference between the results due to rational and irrational ratios λ_1/λ_2 will be discussed briefly in a section later on here, where results are given showing that it makes no difference.

An investigation that is very relevant to the present work is that by Gordillo *et al.* [12] who calculated the phase diagram of a continuous system of bosons in a BCOL. By keeping the interaction strength fixed, the superfluid fraction has been examined as a function of the secondary-OL depth for several values of the primary-OL depth within a range of amplitudes which is larger than ours. It must be emphasized that these authors used a rational approximation to an *irrational* ratio of λ_1 and λ_2 and it has been argued that this is "common practice" [20, 23]. Among their findings, it has been demonstrated that changes in the secondary OL influence the properties and that an MI can be realized. In contrast, the present work conducts a similar investigation chiefly by varying the interaction strength in a *shallow* BCOL with a *rational* λ_1/λ_2 in a regime of interactions near the SG transition, although it is argued that this ratio can also arise from an approximation to the irrational one. It has been found that under these conditions, the properties of bosons are not influenced by changes in the intensity of the secondary OL. Our studies therefore complement the work of Gordillo *et al.*, and are further substantiated with the examination of the SG transition. Moreover, for a strong BCOL additionally considered, changes in the properties can be observed as one varies the intensity of the secondary OL bringing this is in line with the results of Gordillo *et al.* [12].

The bosons in the BCOL are simulated using the continuous−space worm algorithm (WA) quantum Monte Carlo approach [53]. It is found that WA reproduces the SG transition accurately and that the interplay of BCOL and interactions has little effect on changing the critical interaction at which this transition occurs. In fact, it shall be reasoned below that the same result could have been obtained by using irrational ratios close to the rational ones. In other results (1) the OBDM of the system displays substantial depletion of the superfluid as it passes through the SG transition; (2) the MGF shows signals for fermionization detected via the correlation function at the origin, $g_2(0)$, when the total interaction energy goes to zero demonstrating perfect antibunching [54]; (3) the secondary OL has been found not to play a role in aiding or preventing the fermionization.

This work provides more clarification for the interplay between interactions and disorder for repulsive bosons in a quasidisordered OL as has been given earlier by Deissler *et al.* [29]. It is believed that this research will be an important contribution to the field of disordered bosons in 1D.

The organization of the present paper is as follows. In Sec. II the method is presented. In Sec. III the WA code is tested for accuracy as applied to the present system. In Sec. IV the results are presented. In Sec. V the issue of a rational and irrational ratio of the BCOL wavelengths is discussed. In Sec.VI the paper concludes with some closing remarks. In Appendix A the WA is briefly described. In Appendices B, C, and D, the $h_2(r)$, $h_1(r)$, and $h_2(r=0)$, given by Eqs.(14) and (16) below, are reexamined for the same systems in Figs. 4, 6, and 7 that display $g_2(r)$, $g_1(r)$ and $g_2(0)$, respectively, given by Eqs.(9) and (15).

II. METHOD

A brief description of the WA applied to the present system is relegated to Appendix A. The simulations have been conducted on the excellent computational cluster of the Max Planck Institute for Physics of Complex Systems in Dresden, Germany. In essence, the present work has been a heavy-computational project with each simulation taking about a week of CPU time to finish.

A. Optical lattice

In order to introduce disorder into the present system, the WA code [55] –originally designed for a homogeneous Bose gas– has been modified by including a BCOL potential of the form

$$V_{OL}(x) \,=\, V_0 \cos^2(\alpha\pi x) \,+\, V_1 \cos^2(\beta\pi x), \qquad (1)$$

where V_0 and V_1 are the primary and secondary OL depths, respectively, and we always consider $V_1 < V_0$. The parameters $\alpha = 2/\lambda_1$ and $\beta = 2/\lambda_2$, with λ_1 and λ_2 the wavelengths, determine the periodicity of the BCOL and such a type of lattice was shown to realize disorder [11, 28]. α and β were set to 0.4 and 1.0, respectively, for a QPOL, and 0.4 and 1.39 for a quasidisordered optical lattice (QDOL).

A measure for the the strength of the BCOL quasidisorder is its standard deviation δV given by

$$\delta V \,=\, \sqrt{\langle V^2\rangle \,-\, \langle V\rangle^2}, \qquad (2)$$

with

$$\langle V\rangle \,=\, \frac{1}{L}\int_0^L V_{OL}(x)dx, \qquad (3)$$

and

$$\langle V^2\rangle \,=\, \frac{1}{L}\int_0^L V_{OL}^2(x)dx. \qquad (4)$$

According to Deissler *et al.* [18], another measure for the disorder strength is given by

$$\Delta \,=\, 0.5 V_1 \epsilon^2 \exp(-2.18/V_0^{0.6}), \qquad (5)$$

and considering the tunneling amplitude between adjacent lattice sites

$$J \,=\, 1.43 V_0^{0.98} \exp(-2.07\sqrt{V_0}), \qquad (6)$$

this allows one to evaluate Δ/J. In (5) and (6), V_0 and V_1 are in units of E_R (see Sec.II E), and $\epsilon = \beta/\alpha$ is the ratio between the wavelengths of the BCOL.

B. Interactions

The interactions between the bosons are accounted for by the exact two-particle density matrix given by (see e.g. Feynman [56])

$$\rho(x_1 - x_2) \,= \\ 1 \,-\, \sqrt{\frac{\tau}{4ma_s^2}}\, \exp\left\{\frac{m}{4\tau}(x_1 - x_2)^2 \,+\, \frac{|x_1| + |x_2|}{a_{1D}} + \right. \\ \left. \frac{\tau}{ma_{1D}^2}\right\}, \qquad (7)$$

where $\tau = \beta/M$ is the "time step", with $\beta = 1/(\widetilde{T}T_d)$, $\widetilde{T}$ being the temperature in units of the degeneracy temperature T_d, $k_B = 1$ Boltzmann's constant, and $m = 0.5$ is the boson mass. Eq.(7) appears in the worm-update probabilities as a multiplicative factor. The interactions are then essentially described by a delta function $g_{1D}\delta(x_1 - x_2)$, where g_{1D} is the interaction parameter.

In Astrakharchik *et al.* [57], g_{1D} is given by

$$g_{1D} \,=\, -\frac{2\hbar^2}{ma_{1D}}, \qquad (8)$$

where $\hbar$ is Planck's constant and a_{1D} the scattering length. Note that although g_{1D} is negative, it does not indicate attraction which in itself is counterintuitive. Essentially, the absolute value of g_{1D} is considered in the present calculations. From Haller *et al.* [5], the Lieb-Liniger parameter is given by $\gamma \,=\, mg_{1D}/(\hbar^2 n_0)$, and therefore from Eq.(8) one gets $\gamma \,=\, -2/(a_{1D}n_0)$. Here $n_0 \,=\, \langle N\rangle/L$ is the average linear density of the system with $\langle N\rangle$ the thermodynamic average of the particle number and L the length of the system.

C. Pair correlation function

The spatially-averaged pair correlation function (SAPCF) for the 1D homogeneous Bose gas is given by

$$g_2(r) \,=\, \frac{1}{L\,n_0^2}\int_0^L dx\, \langle\hat\psi^\dagger(x+r)\hat\psi^\dagger(x)\hat\psi(x)\hat\psi(x+r)\rangle. \qquad (9)$$

where r is the distance between any two particles along the system and $\hat\psi(x)$ [$\hat\psi^\dagger(x)$] the field operator annihilating [creating] a boson at position x. It can account for the spatially averaged density-density correlation function, given by

$$n_c(r) \,=\, \frac{1}{L}\int_0^L dx\, \langle\hat n(x+r)\hat n(x)\rangle \qquad (10)$$

where $\hat n(x) = \hat\psi^\dagger(x)\hat\psi(x)$ is the density operator. This is because the pair correlations $\langle\hat\psi^\dagger(x+r)\hat\psi^\dagger(x)\hat\psi(x)\hat\psi(x+$

$r)\rangle$ are obtainable from the density-density correlations $\langle\hat{n}(x+r)\hat{n}(x)\rangle$ via the commutator $[\hat{\psi}(x),\hat{\psi}^\dagger(x')] = \delta^{(3)}(x-x')$ [58]

$$\langle\hat{\psi}^\dagger(x+r)\hat{\psi}(x+r)\hat{\psi}^\dagger(x)\hat{\psi}(x)\rangle = \langle\hat{\psi}^\dagger(x+r)\hat{\psi}^\dagger(x)\hat{\psi}(x+r)\hat{\psi}(x)\rangle + \langle\hat{\psi}^\dagger(x+r)\hat{\psi}(x)\rangle\delta^{(3)}(r) \tag{11}$$

so that

$$n_c(r) = g_2(r)n_0^2 + \frac{1}{L}\delta^{(3)}(r)\int_0^L dx\langle\hat{\psi}^\dagger(x+r)\hat{\psi}(x)\rangle. \tag{12}$$

It must be noted that for a translationally invariant system, Eq.(9) reduces effectively to $\langle\hat{\psi}^\dagger(x+r)\hat{\psi}^\dagger(x)\hat{\psi}(x)\hat{\psi}(x+r)\rangle/n_0^2$ and is the same for all x. Therefore by integrating over all x for a translationally invariant system, we average the latter over all the variations with x. On the other hand, when $g_2(r)$ is normalized by the convolution of two spatially-varying densites, $\rho(x)$ and $\rho(x+r)$, that is

$$\rho_c(r) = \frac{1}{L}\int_0^L dx\rho(x+r)\rho(x) \tag{13}$$

instead of n_0^2, where $\rho(x) = \langle\hat{\psi}^\dagger(x)\hat{\psi}(x)\rangle$, one gets the SAPCF for an inhomogeneous BEC given by [59, 60]

$$h_2(r) = \frac{\int_0^L dx\,\langle\hat{\psi}^\dagger(x+r)\hat{\psi}^\dagger(x)\hat{\psi}(x)\hat{\psi}(x+r)\rangle}{\int_0^L dx\,\rho(x+r)\rho(x)}. \tag{14}$$

The examination of $h_2(r)$ is relegated to Appendix B.

D. One-body density matrix

The spatially-averaged one-body density matrix (SA-OBDM) for the 1D homogeneous Bose gas is defined as

$$g_1(r) = \frac{1}{L\,n_0}\int_0^L dx\,\langle\hat{\psi}^\dagger(x+r)\hat{\psi}(x)\rangle, \tag{15}$$

and again for the inhomogeneous case [60]

$$h_1(r) = \frac{\int_0^L dx\,\langle\hat{\psi}^\dagger(x+r)\hat{\psi}(x)\rangle}{\rho_{c,\frac{1}{2}}(r)}. \tag{16}$$

where

$$\rho_{c,\frac{1}{2}}(r) = \frac{1}{L}\int_0^L dx\sqrt{\rho(x+r)\rho(x)} \tag{17}$$

Eq.(15) is used with the same purpose of comparison as in Sec.(II C). The examination of $h_1(r)$ is also relegated to Appendix C. $\rho_c(r)$ and $\rho_{c,\frac{1}{2}}(r)$ will be from now on referred to as the "convoluted densities". In passing, it must be noted that the normalization by n_0^2 in $g_2(r)$, and by $\rho_c(r)$ in $h_2(r)$, just remains a matter of convenience regarding what purpose each one would achieve. For $g_2(r)$ this simply entails information about the density-density correlations and stronger signals than $h_2(r)$. For $g_1(r)$ and $h_1(r)$ it turns out that the normalization by n_0 and $\rho_{c,\frac{1}{2}}(r)$, respectively, doesn't make much difference. It must be added that experimentally one favors measuring the spatially-integrated correlation functions, Eqs.(9) and (15), because otherwise it requires a lot of data to determine the dependence of the correlations on two coordinates, a fact that has been stated earlier by Naraschewski et al. [60].

E. Units and parameters

The degeneracy temperature is given by $T_d = 2\pi\hbar^2 n_0^2/m$, and the photon recoil energy by $E_R = h^2/(2m\lambda^2)$; their ratio is always $T_d/E_R = 4/\pi$. Here λ is the wavelength of the laser beams creating the OL where $\lambda = 2d$ is twice the lattice period d [$= 1/\alpha$; cf. Eq.(1)] and $n_0 = 2/\lambda$ is the average linear density. Hence, an OL depth like, e.g., 1.0 in units of E_R corresponds to $V_0 = 1.0\,E_R/T_d = 1.0\times\pi/4 = 0.785$ in units of T_d. Now in the WA code the mass is $m = 0.5$, $\hbar = 1$, $\lambda/L = 0.01$, and $n_0\lambda = 2.0$, and therefore $T_d = 4\pi n_0^2 = 0.64\pi$ and $E_R = 4\pi^2\hbar^2/(2m\lambda^2) = 0.16\pi^2$. It should be emphasized that T_d is computed from an initial density parameter n_0 that is only used to fix the size of the system and that is not updated during the simulations. That is, the final density of the system n can be different from the initial n_0. However, in the present simulations n_0 is equal to n and the temperature is set to $\widetilde{T} = T/T_d = 0.001$ to allow a significant value of ρ_s/ρ.

The length of the system is such that $2L/\lambda = 200$ lattice sites and is at almost perfect commensurate filling. For purposes of comparison, the value of the wavelength is the same as that used by Haller *et al.* [5], namely $\lambda = 1064.5$ nm and the values for the OL depth V_0 are of the same order of magnitude as in Haller *et al.* [5] and Gordillo *et al.* [12]. In [12], the wavelength of the laser beams generating the OL was $\lambda = 830$ nm and considering that the 3D scattering length of Rb^{87} is almost $100a_0$, the 1D Lieb-Liniger interaction parameter becomes $\gamma = 1.770$. The values of γ used in the present work are in general larger than in Ref. [12] as they extend into the strongly interacting SG regime.

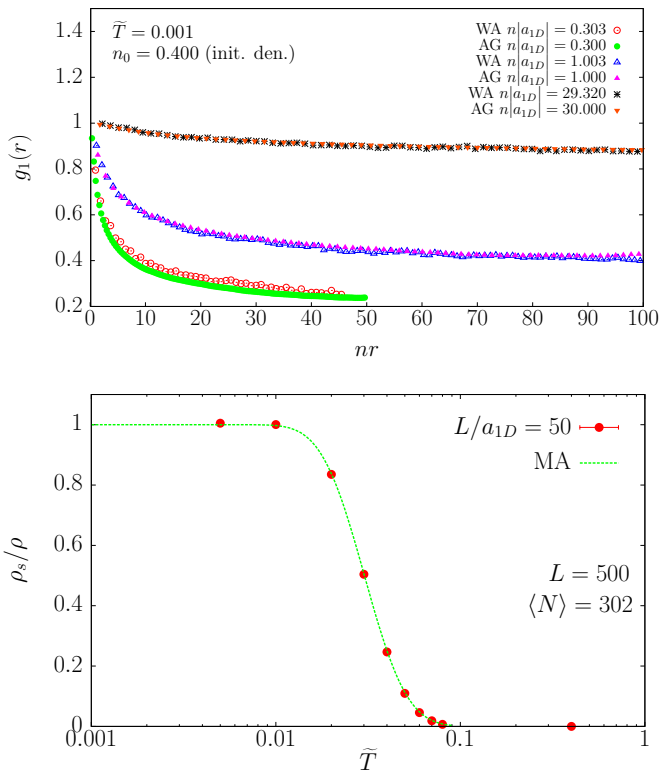

FIG. 1: (Color online) Upper frame: WA first order correlation function $g_1(r)$ (one-body density matrix) as a function of nr for several parameters $n|a_{1D}|$ compared to results from Astrakharchik and Giorgini (AG) [57] for values of $n|a_{1D}|$ which are almost identical to the WA ones. The system is a 1D homogeneous Bose gas at a temperature of $\widetilde{T} = 0.001$. Here n is the average linear density and a_{1D} the 1D scattering length. For the WA we have: $n|a_{1D}| = 0.303$ (open circles), 1.003 (open up triangles), and 29.320 (stars), respectively. The corresponding data from AG are for almost the same $n|a_{1D}|$: 0.300 (solid circles), 1.000 (solid up triangles), and 30.000 solid down triangles, respectively. $\widetilde{T}$ is in units of the transition temperature T_d and the initial density of the simulation is $n_0 = 0.4$. Lower frame: Superfluid fraction ρ_s/ρ as a function of temperature $\widetilde{T}$. The system is again a 1D homogeneous gas of Bosons. The scattering length is $a_{1D}/L = 1/50$, the length of the system is $L/a_{1D} = 50$ and the thermodynamic average of the number of particles is $\langle N \rangle = 302$. The solid circles are the WA results whereas the solid line is an analytical calculation using Eq.(18) of Del Maestro and Affleck [61] with the same parameters as ours (see text).

III. TESTS OF THE WA CODE

In this section the WA code [55] is tested on a uniform interacting Bose gas in the absence of any trapping potential. First, it is verified that the code produces the OBDM properly via a comparison with previous results. Second, it is confirmed that for suitably chosen parameters, the temperature of the simulations is low enough to obtain a significant superfluid fraction ρ_s/ρ. In this respect, WA results for ρ_s/ρ as a function of $\widetilde{T}$ were found to exactly match an analytical calculation. In another decisive program check, although this is implied in the subsequent Sec. IV A, the SG transition originally observed by Haller *et al.* [5] was reproduced by adding a shallow periodic 1D OL to the homogeneous Bose-gas system.

A. One-body density matrix

The upper frame of Fig. 1 displays the OBDM $g_1(r)$ as a function of nr at various $n|a_{1D}|$ obtained from WA simulations for three of the homogeneous Bose-gas cases already considered by Astrakharchik and Giorgini (AG) [57]. The values of $n|a_{1D}|$ range from the strongly to the weakly-interacting regime as $n|a_{1D}|$ is increased. One can see that the agreement is excellent.

B. Superfluid fraction

The lower frame of Fig. 1 displays a comparison between the superfluid fraction ρ_s/ρ obtained by WA and that by the equation

$$\rho_s/\rho \;=\; 1 \;-\; u \left| \frac{\theta_3''(0, e^{-2\pi u})}{\theta_3(0, e^{-2\pi u})} \right| \qquad (18)$$

that is the same as Eq.(16) of Ref.[61]; except that it is rescaled to our units. Here $u = 1/(2\widetilde{T}\langle N \rangle)$, with $\widetilde{T} = T/T_d$, $\langle N \rangle = 302$, and $L/a_{1D} = 50$. θ_3 is the Jacobi Theta function of the third kind given by

$$\theta_3(z, q) \;=\; \sum_{n=-\infty}^{+\infty} q^{n^2} \exp(i2nz), \qquad (19)$$

and can be evaluated using WOLFRAM MATHEMATICA®. The system is a weakly interacting, dilute, and uniform 1D Bose gas whose initial density was set to $n_0 = 0.2$ so that $T_d = 0.5027$. The WA results match exactly those of the analytical Eq.(18) casting away all doubts about the accuracy of the WA code. Further, $\widetilde{T} = 0.001$ is low enough to allow a significant value for ρ_s/ρ. The reader must be alerted, that the parameters used in this section and the previous one are only for the purpose of making the comparisons in Fig. 1. The rest of this paper uses the parameters of Sec. II E above.

C. Chemical potential and interactions

In the simulations below, the number of particles N for each γ was fixed extremely close to 200 by a careful tuning of the chemical potential μ from a calibration curve, i.e., a plot of N versus μ for each interaction

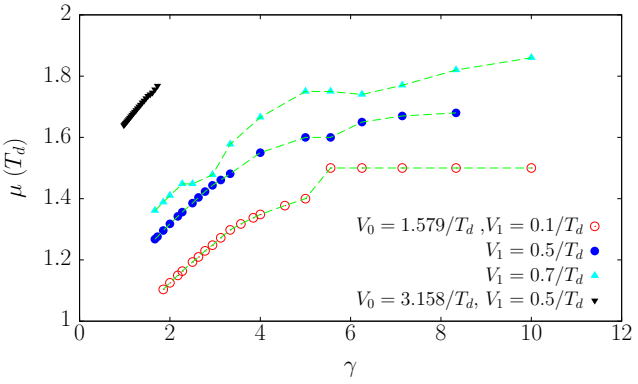

FIG. 2: (Color online) Calibrated chemical potential μ as a function of γ for the commensurate filling of a number of BCOLs with $\alpha = 0.4$ and $\beta = 1.0$ at $N = 200 \pm \delta$ particles, where δ is a small error. The figure displays the case for $V_0 = 1.579/T_d$ and $V_1 = 0.1/T_d$ (open circles); $0.5/T_d$ (solid circles); $0.7/T_d$ (solid up triangles); and then the case for $V_0 = 3.158/T_d$ and $V_1 = 0.5/T_d$ (solid down triangles). μ is in units of T_d and γ is unitless.

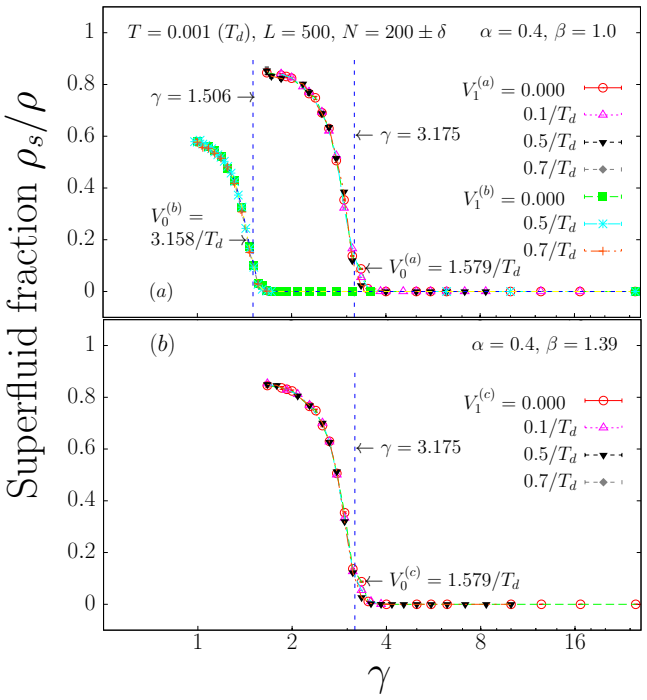

FIG. 3: (Color online) WA superfluid fraction ρ_s/ρ versus the Lieb-Liniger parameter γ for an interacting Bose gas in several realizations of the BCOL. The figure demonstrates primarily the WA numerical reproduction of the Sine-Gordon transition observed experimentally in Ref.[5]. The temperature of the system is $\widetilde{T} = 0.001$, its length L is such that $2L/\lambda = 200$, and the number of particles N is very close to 200 with a small error δ that is within the range ± 1. Two primary OL depths $V_0^{(a)} = 1.579/T_d$ and $V_0^{(b)} = 3.158/T_d$ are considered with different associated depths $V_1^{(a)}$ and $V_1^{(b)}$ of the superimposed secondary OLs, respectively. Each of the primary OLs has exactly 200 sites with an occupancy of one particle per site in the SG regime. Upper frame (a) is for a QPOL with $\alpha = 0.4$ and $\beta = 1.0$. Open circles: $V_1^{(a)} = 0.000$ (purely periodic OL); open up triangles: $0.1/T_d$; solid down triangles: $0.5/T_d$; and solid diamonds: $0.7/T_d$. Solid squares: $V_1^{(b)} = 0.000$; stars: $0.5/T_d$; and crosses: $0.7/T_d$. Lower frame (b) is for a quasidisordered OL with $V_0^{(c)} = 1.579/T_d$, the same α, but a different $\beta = 1.39$. The labels for $V_1^{(c)}$ are the same as for $V_1^{(a)}$. The vertical dashed lines show the SG transition points $\gamma = 3.175$ for $V_0^{(a)} = V_0^{(c)} = 1.579/T_d$, and 1.506 for $V_0^{(b)} = 3.158/T_d$ which are very close to the ones found on the phase diagram Fig.3 of Haller *et al.* [5]. V_0, V_1, and $\widetilde{T}$ are in units of T_d and γ is unitless.

strength γ. The error bars δ in N were within ± 1.0 and this error is unavoidable as one is dealing with a continuous-space Monte Carlo simulation. Fig. 2 displays a plot of the calibrated μ versus γ for a number of BCOL realizations. The μ rises in general with γ until it begins to stabilize in the strongly-interacting SG regime.

IV. RESULTS

A. Sine-Gordon transition

An important result of this work is that the WA is able to reproduce the SG transition [5] in a primary 1D shallow periodic OL. It is found that the latter transition is robust against perturbations arising from the addition of a weaker secondary OL. The critical value γ_c at which the transition occurs in a BCOL (1) remains exactly the same as compared to a periodic OL with the same V_0, unaffected by the latter perturbations. This is the chief result of this paper and is demonstrated by the behavior of ρ_s/ρ as a function of γ for a Bose gas in various realizations of a 1D BCOL (1). Fig. 3 demonstrates this finding for two values of the primary depth $V_0^{(a)}$ and $V_0^{(b)}$ and different strengths of the associated secondary OL, $V_1^{(a)}$ and $V_1^{(b)}$, respectively. Here, ρ_s/ρ displays a steep decline towards the critical γ_c beyond which it remains zero deep into the SG regime $\gamma \gg \gamma_c$. The value of γ_c indicated by a vertical dashed line is obtained by fitting a function of the form $f(\gamma) = A(\gamma - \gamma_c)^s$ to the data of ρ_s/ρ in a narrow range of γ where ρ_s/ρ comes close to zero. Here A, γ_c, and s are fitting parameters. We shall return to this issue in a future publication where a comparison between WA numerical and experimental results is required in order to explore the validity of the SG theory [62]. The addition of a secondary OL does not alter the behavior of ρ_s/ρ from the one observed for $V_1^{(a,b,c)} = 0$, the purely periodic OL. For $V_0^{(c)} = 1.579/T_d$, the behavior of ρ_s/ρ in frame (b) with $\beta/\alpha = 3.475$ is exactly the same as in frame (a) with $\beta/\alpha = 2.5$ and the same $V_0^{(a)} = 1.579/T_d$. This is a rather peculiar result showing that an increased quasidis-

TABLE I: Ratio between the disorder strength Δ [Eq.(5)] and the tunneling amplitude J [Eq.(6)] for various realizations of the BCOL. The table lists from left to right the primary OL depth V_0, the secondary one V_1, the parameters determining the periodicity of the BCOL (1), α and β, the parameters Δ and J, and then Δ/J. The OL depths are in units of T_d, whereas Δ and J are in units of E_R.

V_0 (T_d)	V_1 (T_d)	α	β	Δ (E_R)	J (E_R)	Δ/J
1.579	0.1	0.4	1.0	0.0224	0.1804	0.1240
	0.5			0.1119	0.1804	0.6200
	0.7			0.1566	0.1804	0.8679
	0.1		1.39	0.0432	0.1804	0.2395
	0.5			0.2161	0.1804	1.1977
	0.7			0.3026	0.1804	1.6768
3.158	0.5		1.0	0.2349	0.1510	1.5553
	0.7			0.3288	0.1510	2.1775
6.316	1.0			0.7662	0.0886	8.6495
	3.0			2.2987	0.0886	25.948
	1.0		1.39	1.4805	0.0886	16.712
	3.0			4.4414	0.0886	50.135

order [cf. Eq.(5) with $\epsilon = \beta/\alpha$] in a shallow BCOL does not alter the behavior of ρ_s/ρ. The values of γ_c at which the transitions occur for both values of V_0 are very close to the ones obtained from the phase diagram in Fig. 3 of Haller *et al.* [5]. This is again a striking demonstration of the fact that the WA is a powerful method enabling an accurate simulation of the behavior of lattice bosons in continuous space.

The robustness of ρ_s/ρ against the secondary-OL perturbations arises because the particles always seek the lowest energy states of the BCOL, i.e., those of the primary OLs. Further, in the strongly-interacting regime $\gamma > 1$, the interactions override the effects introduced by V_1 as the behavior of bosons is chiefly dictated by the commensurate filling of the primary OL. This finding is brought in line with that of Boeris *et al.* [16], who argued that in the limit of a shallow periodic potential the optical depth becomes subrelevant when the Mott transition is only controlled by interactions.

B. Effect of secondary lattice

Figure 4 shows the influence of V_1 on the spatial behavior of $g_1(r)$ and $g_2(r)$, particularly the amplitudes of the $g_2(r)-$oscillations, for various realizations of the BCOL. A significant feature is that $g_2(r)$ reveals a spatial oscillatory structure whose origin can be traced back to the primary OL. On the other hand, $g_1(r)$ in (C) displays a structure similar to $g_1(r)$ of the 1D homogeneous Bose gas in Fig. 1 without any spatial oscillations.

As V_0 is increased, so do the oscillatory amplitudes of $g_2(r)$ in (B) displaying its deep connection to the OL. An enhanced spatial decay rate of $g_1(r)$ at larger V_0 in (C) indicates a reduction of the superfluid fraction. The spatial frequency of the $g_2(r)-$oscillations neither changes with V_0 nor with V_1, and is largely governed by the lattice parameter of the primary OL. When V_0 and V_1 are small, e.g. $\sim 1.5/T_d$ in frames (A) and (C), a change of V_1 does not alter the spatial behavior. Remarkably, the secondary OL is practically not "seen" by the bosons in this case. The $g_1(r)$ and $g_2(r)$ for bosons in a QPOL ($\beta = 1.0$) do not differ from those in a QDOL ($\beta = 1.39$). However, when V_0 is increased to larger values $\sim 6/T_d$ as in (B) and (D), a change in the band structure of the BCOL via V_1 and β begins to assert itself in $g_2(r)$ and $g_1(r)$. Further, at larger $V_0 = 6.316/T_d$, the change in the oscillatory amplitude of $g_2(r)$ with V_1 is more pronounced for a QPOL than for a QDOL indicating that an increased disorder does not necessary yield a stronger response to V_1. The same argument can be applied to $g_1(r)$ in frame (D). The secondary OL begins to influence the properties only in conjunction with a larger V_0 at which the BCOL begins to compete with the boson-boson interactions. Indeed, the difference in β/α introduces a difference between the band structures of the QPOL and the QDOL and therefore the corresponding $g_2(r)$.

One can also explain the stronger response to V_1 by examining Δ/J for a noninteracting Bose gas in a BCOL. A plot of Δ/J [cf. Eqs.(5) and (6)] as a function of V_0, shows that Δ/J increases significantly at the larger V_1. Naturally, according to Eq.(5), Δ rises with ϵ and V_1. Fig. 5 demonstrates these facts for a number of V_1 values and for $\alpha = 0.4$ and $\beta = 1.0$ only. In addition, Table I lists Δ/J for the various realizations of the BCOL in the present work. It can be seen for example that for $V_0 = 6.316/T_d$ and $\beta = 1.39$, Δ/J begins to attain values that are much larger than for the rest of the BCOL parameters. As such, the properties of the system should begin to change significantly at this V_0-height. For the other OL depths and $\beta-$values, Δ/J has relatively small values of the order of ~ 1, and therefore, the secondary OL is unable to cause any changes in the properties.

C. Effect of interactions on the correlations

Fig. 6 demonstrates the effect of interactions on $g_2(r)$ for all realizations of the BCOL. The qualitative pattern of these oscillations hardly changes with γ (and V_1), even on going through the SG transition. Quantitatively, however, the amplitude of these oscillations rises in general in response to an increase of γ (and V_0). [Compare frame (c) with both (a) and (b).] The latter manifests an increase in the interplay between the interactions and the BCOL that in turn enhances the boson-boson (i.e., density-density $n_c(r)$) correlations. It must be emphasized that the rise in the amplitude of $g_2(r)-$oscillations is particularly significant beyond γ_c reaching deep into the SG regime where the bosons are pinned. This is

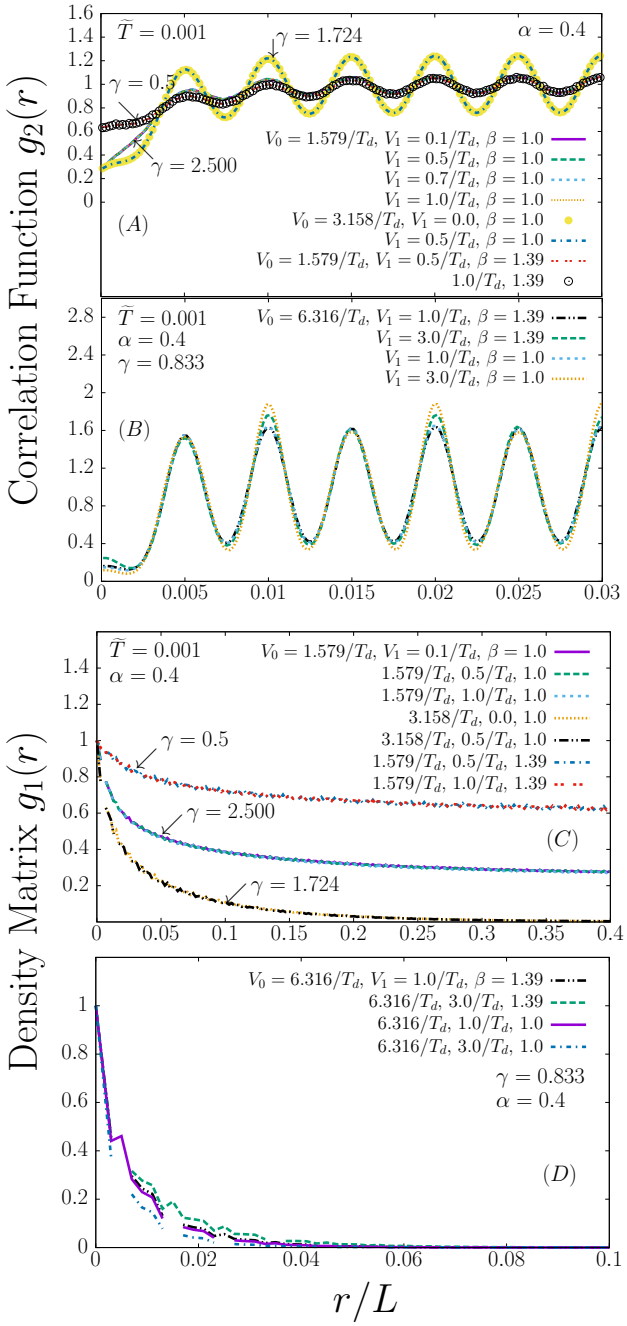
Correlation Function $g_2(r)$
Density Matrix $g_1(r)$
r/L
$\bar{T} = 0.001$
$\alpha = 0.4$
$\gamma = 1.724$
$\gamma = 0.5$
$\gamma = 2.500$
(A)
$V_0 = 1.579/T_d$, $V_1 = 0.1/T_d$, $\beta = 1.0$
$V_1 = 0.5/T_d$, $\beta = 1.0$
$V_1 = 0.7/T_d$, $\beta = 1.0$
$V_1 = 1.0/T_d$, $\beta = 1.0$
$V_0 = 3.158/T_d$, $V_1 = 0.0$, $\beta = 1.0$
$V_1 = 0.5/T_d$, $\beta = 1.0$
$V_0 = 1.579/T_d$, $V_1 = 0.5/T_d$, $\beta = 1.39$
$1.0/T_d$, 1.39
$\bar{T} = 0.001$
$\alpha = 0.4$
$\gamma = 0.833$
$V_0 = 6.316/T_d$, $V_1 = 1.0/T_d$, $\beta = 1.39$
$V_1 = 3.0/T_d$, $\beta = 1.39$
$V_1 = 1.0/T_d$, $\beta = 1.0$
$V_1 = 3.0/T_d$, $\beta = 1.0$
(B)
$\bar{T} = 0.001$
$\alpha = 0.4$
$V_0 = 1.579/T_d$, $V_1 = 0.1/T_d$, $\beta = 1.0$
1.579/T_d, 0.5/T_d, 1.0
1.579/T_d, 1.0/T_d, 1.0
3.158/T_d, 0.0, 1.0
3.158/T_d, 0.5/T_d, 1.0
1.579/T_d, 0.5/T_d, 1.39
1.579/T_d, 1.0/T_d, 1.39
$\gamma = 0.5$
$\gamma = 2.500$
$\gamma = 1.724$
(C)
$V_0 = 6.316/T_d$, $V_1 = 1.0/T_d$, $\beta = 1.39$
6.316/T_d, 3.0/T_d, 1.39
6.316/T_d, 1.0/T_d, 1.0
6.316/T_d, 3.0/T_d, 1.0
$\gamma = 0.833$
$\alpha = 0.4$
(D)

FIG. 4: (Color online) Effect of secondary optical lattice on the spatially-averaged correlation function $g_2(r)$ [Eq.(9)] and the spatially-averaged density matrix $g_1(r)$ [Eq.(15)] of the systems in Fig. 3. Here r is the distance between any pair of particles along the lattice and all frames share the same $x-$axis label. Frame (A) shows $g_2(r)$ for $\alpha = 0.4$ at different interaction strengths and for various BCOL realizations. For $\gamma = 2.500$, $V_0 = 1.579/T_d$, and $\beta = 1$, the figure displays the cases for: $V_1 = 0.1/T_d$ (solid line); $0.5/T_d$ (long-dashed line); $0.7/T_d$ (short-dashed line); $1.0/T_d$ (fine-dotted line). (It is difficult to plot these lines so that all symbols can be distinguished from each other because they're exactly overlapping. The same applies to the rest of the plots.) For $\gamma = 1.724$, $V_0 = 3.158/T_d$, and the same β, the figure shows the cases for $V_1 = 0.0$ (solid circles) and $0.5/T_d$ (dashed-dotted line). The last set of data is for $\gamma = 0.5$, $V_0 = 1.579/T_d$ but with $\beta = 1.39$ and: $V_1 = 0.5/T_d$ (double-dotted line) and $1.0/T_d$ (open circles). Frame (B) is as in (A); except for $V_0 = 6.316/T_d$, $\gamma = 0.833$, and: $V_1 = 1.0/T_d$ with $\beta = 1.39$ (dashed double-dotted line); $3.0/T_d$ with 1.39 (long-dashed line); $1.0/T_d$ with 1.0 (short-dashed line); and $3.0/T_d$ with 1.0 (fine-dotted line). Going over to $g_1(r)$, frame (C) displays it for $\gamma = 2.500$, $V_0 = 1.579/T_d$, and: $V_1 = 0.1/T_d$ with $\beta = 1.0$ (solid line); $0.5/T_d$ and 1.0 (dashed line); $1.0/T_d$ and 1.0 (dotted line). The following set of data is for $\gamma = 1.724$, $V_0 = 3.158/T_d$ and: $V_1 = 0.000$ with $\beta = 1.0$ (fine-dotted line); $0.5/T_d$ with $\beta = 1.0$ (dashed double-dotted line). Next comes $V_0 = 1.579/T_d$, $\gamma = 0.5$, and $V_1 = 0.5/T_d$ with $\beta = 1.39$ (dashed-dotted line); $1.0/T_d$ and 1.39 (double-dotted line). Finally, frame (D) is as in (C); except for $V_0 = 6.316/T_d$, $\gamma = 0.833$, and: $V_1 = 1.0/T_d$ with $\beta = 1.39$ (dashed double-dotted line); $3.0/T_d$ and 1.39 (dashed line); $1.0/T_d$ and 1.0 (solid line); $3.0/T_d$ and 1.0 (dashed-dotted line). The r is in units of L, $\bar{T}$ is in units of T_d, and γ is unitless.

therefore indicative of a Mott insulator (MI) state which is not inert. An examination of the MGF $G(p = 0, \tau)$ in Sec. IV G and by making connections to $g_2(r)$, it is inferred that holes, arising from particle-hole (p−h) excitations, play an important role in the enhancement of $g_2(r)$.

On the one hand, the response of $g_2(r)$ to γ can be further clarified by other arguments. First, it is known that $g_2(r)$ [Eq.(9)] describes the probability of finding two particles at a separation r. Hence, as the bosons become more localized with increasing γ, the probability –i.e., the amplitude of $g_2(r)-$oscillations– rises. Second, when the interactions are large, higher harmonics in the density operator $\widetilde{\rho}(x)$ from Ref.[7] become excited that play a role in intensifying $g_2(r)$. Here, $\psi(x) = \sqrt{\widetilde{\rho}(x)}\exp(i\varphi(x))$ is a field operator with $\varphi(x)$ a phase and [7, 19]

$$\widetilde{\rho}(x) = \left\{ n^2 + \frac{1}{\pi^2}[\nabla\phi(x)]^2 + n^2 \sum_{p>1} \cos(2\pi n x - 2p\phi(x)) \right\}^{1/2} \tag{20}$$

where $\phi(x)$ is a boson field operator and n the average

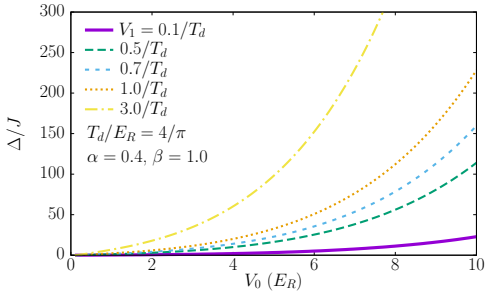

FIG. 5: (Color online) Δ/J [given by Eqs.(5) and (6)] as a function of the primary OL depth V_0 for various values of V_1: $0.1/T_d$ (solid line); $0.5/T_d$ (long-dashed line); $0.7/T_d$ (short-dashed line); $1.0/T_d$ (dotted line); and $3.0/T_d$ (dashed double-dotted line). The conversion factor from units of T_d to E_R is $T_d/E_R = 4/\pi$, V_0 is in units of E_R, and Δ/J is unitless.

density. On the other hand, the rise in the amplitude with V_0 can be related to the amplitude of the Wannier state in each OL well. For sufficiently deep OLs, the Wannier state can be approximated by a harmonic oscillator ground state [51]

$$W(x) = \frac{k^{1/2}}{\pi^{1/4}}\left(\frac{V_0}{E_r}\right)^{1/8}\exp\left[-\frac{1}{2}\left(\frac{V_0}{E_r}\right)^{1/2}k^2x^2\right] \tag{21}$$

where k is the primary lattice wavevector. The amplitude of $W(x)$ rises with V_0 at each lattice site and consequently the amplitude of $g_2(r)$. Moreover, it has been found [63], that correlations arise from the interplay of quantum statisics, interactions, thermal, and quantum fluctuations, the last of which can be related to the higher harmonics in Eq.(20).

D. Another test of the WA for $g_2(r)$

For the homogeneous Bose gas, we display in Fig. 6(c) the analytic result for $g_2(r)$ perturbative in $1/\gamma$ [54]

$$g_2^{(per)}(z,1/\gamma) = 1 - \frac{\sin^2 z}{z^2} - \frac{4}{\gamma}\frac{\sin^2 z}{z^2} - \frac{2\pi}{\gamma}\frac{\partial}{\partial z}\frac{\sin^2 z}{z^2} + \frac{2}{\gamma}\frac{\partial}{\partial z}\left[\frac{\sin^2 z}{z^2}\int_{-1}^{1} dt\,\sin(zt)\ln\frac{1+t}{1-t}\right] \tag{22}$$

where $z = n\pi r$ and the one perturbative in γ

$$g_2^{(per)}(r,\sqrt{\gamma}) = 1 - \sqrt{\gamma}\left[\mathrm{L}_{-1}\left(2\sqrt{\gamma}nr\right) - \mathrm{I}_1\left(2\sqrt{\gamma}nr\right)\right], \tag{23}$$

where, $\mathrm{L}_{-1}(x)$ and $\mathrm{I}_1(x)$ are the Struve and Bessel functions, respectively. Eq.(22) is plotted with $\gamma = 10$ for the strongly, whereas (23) with $\gamma = 0.1$ for the weakly interacting regime. The goal is to check the WA $g_2(r)$

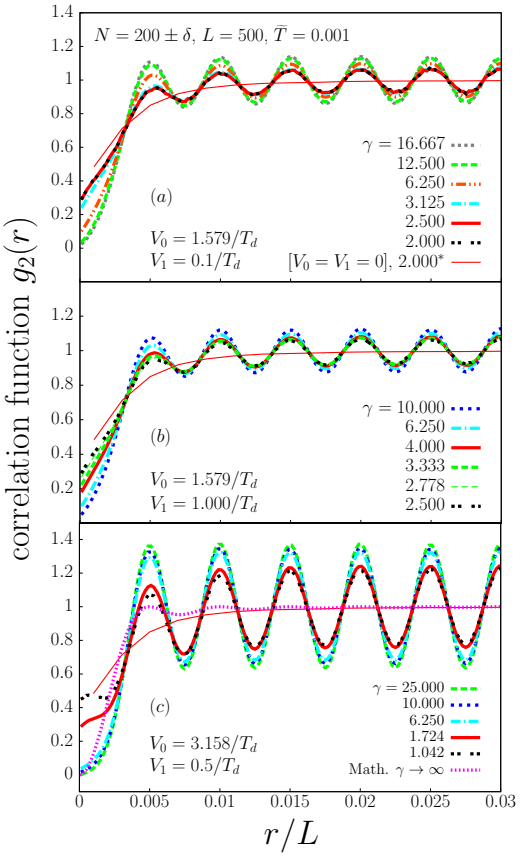

FIG. 6: (Color online) WA pair correlation function $g_2(r)$ [Eq.(9)] at various interactions γ for the systems of Fig. 3(a) and three realizations of the BCOL with $\alpha = 0.4$ and $\beta = 1.0$. Frame (a) is for the BCOL of primary depth $V_0 = 1.579/T_d$ and a secondary depth $V_1 = 0.1/T_d$ at $\gamma = 16.667$ (dotted line); 12.500 (dashed line); 6.250 (dashed triple-dotted line); 3.125 (dashed-dotted line); 2.500 (thick solid line); and 2.000 (double-dotted line). For additional comparison, the thin solid line is exceptionally displayed for a homogeneous Bose gas without an OL [$V_0 = V_1 = 0$] at $\gamma = 2.000$ and the same parameters as in Fig. 3(a). It is also displayed in frames (b) and (c). Frame (b) is as in (a); but for $V_1 = 1.0/T_d$ and $\gamma = 10.000$ (dotted line); 6.250 (dashed-dotted line); 4.000 (thick-solid line); 3.333 (dashed line); 2.778 (thin-dashed line); 2.500 (double dotted line). Frame (c) is for $V_0 = 3.158/T_d$, $V_1 = 0.5/T_d$, and: $\gamma = 25.000$ (dashed line); 10.000 (dotted line); 6.250 (dashed-dotted line); 1.724 (thick solid line); 1.042 (double-dotted line). The fine-dotted line shows the pair correlation function. The thin-dashed and thin-dashed-dotted lines show the analytic results $g_2^{(per)}(z,1/\gamma)$ with $z = n\pi r$ [Eq.(22)] at $\gamma = 10$ and $g_2^{(per)}(r,\sqrt{\gamma})$ [Eq.(23)] at $\gamma = 0.1$ from Ref.[54]. The plot for these functions was generated by Mathematica®. There is almost perfect commensurate filling with $N = 200 \pm \delta$ particles, where δ is a small error in the range ± 1. V_0, V_1, and $\widetilde{T}$ are in units of T_d, and γ is unitless.

[e.g. for $\gamma = 2.000$] without an OL against analytic calculations, and one can see that the WA result lies largely intermediate between these analytic results. This shows again that WA is reliable in calculating these properties.

E. Origin of oscillations

Despite the fact that (22) diplays weak oscillations, these are substantially enhanced in the WA $g_2(r)$ by the addition of an OL. The WA $g_2(r)$ for the Bose gas without an OL does not show any oscillations whatsoever [e.g. for $\gamma = 2.000$ and no OL in Fig. 6]. It is known that strongly-repulsive bosons in 1D without an OL arrange themselves in a periodic structure as if they were ordered inside an OL, but still the $g_2(r)$ reveals no spatial oscillations. Fact is, that the OL introduces a different energy level structure that reshapes the wavefunction into a spatially oscillatory form.

Let us here only mention briefly the results of the appendices and the reader is referred to the them for more information. In Appendix B, the SAPCF $h_2(r)$ [Eq.(14)] and the SA-OBDM $h_1(r)$ [Eq.(16)] are displayed in Figs. 9 and 10 (for the same systems of Figs. 4 and 6, respectively). The goal is to reveal the effects introduced into the correlations when instead of n_0^2 and n_0, the $g_2(r)$ and $g_1(r)$ are normalized by $\rho_c(r)$ and $\rho_{c,\frac{1}{2}}(r)$ [Eq.(13) and (17)], respectively. [That is $g_1(r) \to h_1(r) = g_1(r)n_0/\rho_{c,\frac{1}{2}}(r)$ and $g_2(r) \to h_2(r) = g_2(r)n_0^2/\rho_c(r)$.] The result is that in general –for a shallow BCOL– $h_2(r)$ displays oscillations with a (much) smaller amplitude than $g_2(r)$. In fact for a shallow BCOL, $h_2(r)$ is seen to approach the behavior of $g_2(r)$ for a homogeneous Bose gas! It can therefore be concluded, that in this case the origin of the $g_2(r)-$oscillations is the oscillations in the spatial density whose structure is determined by the OL. In Appendix B, except for small oscillations, $h_1(r)$ shows generally the same qualitative behavior as $g_1(r)$.

F. Interaction energy and local $g_2(0)$

According to Astrakharchik *et al.* [57], the total interaction energy E_{int} can be computed from $g_2(r)$ at $r = 0$ using

$$\frac{E_{int}}{\langle N \rangle T_d} = \frac{1}{2} g_{1D} n g_2(0). \tag{24}$$

Now E_{int} goes to zero as γ is increased to large values beyond γ_c because $g_2(0) \to 0$. This can be seen in Fig. 6 for $\gamma > 6.250$ in all frames and is a stark indication to fermionization of the bosons [64] and demonstrates perfect antibunching [54]. In frame (c), fermionization is reached at $\gamma = 10$ whereas in frames (a) and (b) it requires $\gamma > 10$. Therefore, a larger V_0 aids the fermionization process of bosons since there is an enhanced effective interaction arising from the interplay between the BCOL and the repulsive forces that reduces the value of γ required for fermionization. The added secondary OL does not play a role in this regard.

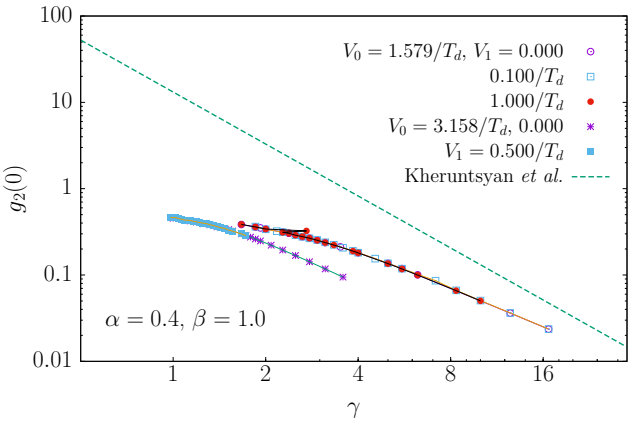

FIG. 7: (Color online) Spatially-averaged WA local pair correlation function $g_2(r = 0)$ [Eq.(9)] as a function of γ for the systems of Fig. 6 in comparison to $g^{(2)}(\gamma)$ of Kheruntsyan *et al.* [64] (dashed line) for the homogeneous Bose gas in the strongly interacting regime $\gamma > 1$. Here, the QPOL is with $\alpha = 0.4$ and $\beta = 1.0$. The figure displays $g_2(0)$ for $V_0 = 1.579/T_d$ with $V_1 = 0$ (open circles); with $V_1 = 0.100/T_d$ (open squares); and with $V_1 = 1.000/T_d$ (solid circles). The stars are for $V_0 = 3.158/T_d$ with $V_1 = 0.000$ and with $V_1 = 0.5/T_d$ (solid squares).

In Fig. 7, $g_2(0)$ is plotted as a function of γ for the two BCOLs with $V_0 = 1.579/T_d$ and $3.158/T_d$ and some values of V_1. For comparison, the analytical result for the homogeneous Bose gas of Ref.[64],

$$g^{(2)}(\gamma) = \frac{4}{3}\frac{\pi^2}{\gamma^2}\left[1 + \frac{t^2}{4\pi^2}\right], \tag{25}$$

with $t = T/T_d$ is displayed by the linear dashed line. It is immediately observed that, whereas on the one hand the introduction of an OL to a homogeneous Bose gas reduces E_{int} via a significant reduction of $g_2(0)$, the addition of a secondary weaker OL does not play much of a role in changing the behavior of $g_2(0)$ for the same V_0. The interaction in the system is therefore not influenced by a perturbation of the primary OL. The effect of γ on $g_1(r)$ shall be explored in a future publication in connection to the change of its behavior across the SG transition.

In Appendix D, $h_2(0)$ vs γ is displayed in Fig. 11 for the same systems of Fig. 7. Peculiarly, $h_2(0)$ shows qualitatively the same behavior of $g_2(0)$.

G. Matsubara Green's function

The MGF $G(p = 0, \tau)$ displays (1) the presence of a gas of particle-hole (p-h) pairs revealing that the insulating state obtained following the SG transition is not

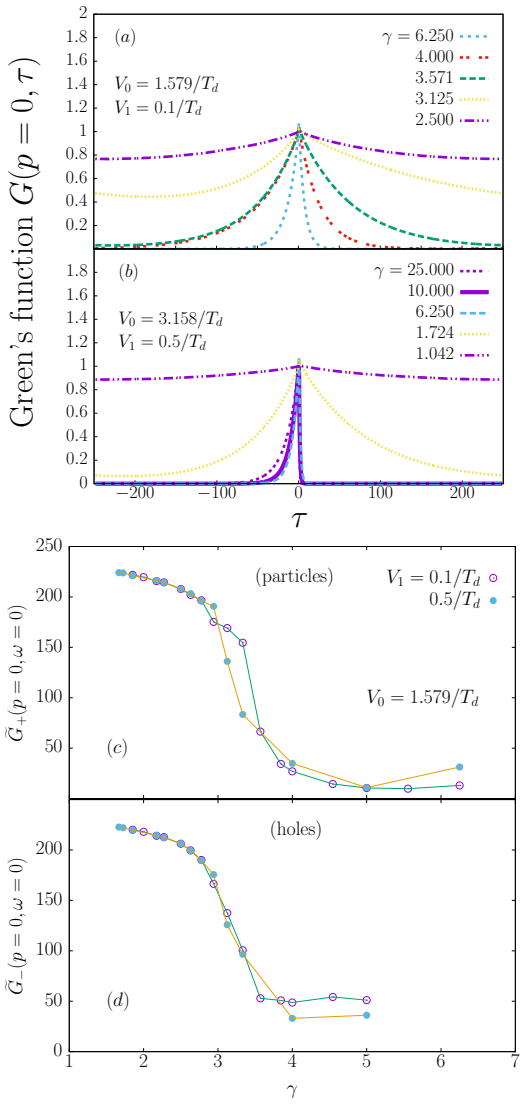

FIG. 8: (Color online) WA Matsubara Green's function $G(p = 0, \tau)$ and weights of particle and hole (p-h) excitations $\widetilde{G}_+(p = 0, \omega = 0)$ and $\widetilde{G}_-(p = 0, \omega = 0)$ [Eq.(29)], respectively, for the systems of Fig. 3. Upper figure displays G as a function of τ for some values of γ, and the lower $\widetilde{G}_\pm$ as a function of γ –all for different values of V_1. Frame (a) displays G for $V_0 = 1.579/T_d$ and $V_1 = 0.100/T_d$ with: $\gamma = 6.250$ (dotted line); 4.000 (double-dotted line); 3.571 (dashed line); 3.125 (fine-dotted line); 2.500 (dashed triple-dotted line). Frame (b) is as in (a); but with $V_0 = 3.158/T_d$, $V_1 = 0.5/T_d$ and: $\gamma = 25.000$ (dotted line); 10.000 (solid line); 6.250 (dashed line); 1.724 (fine-dotted line); 1.042 (dashed triple-dotted line). Frame (c) shows $\widetilde{G}_+$ for $V_0 = 1.579/T_d$ and $V_1 = 0.1/T_d$ (open circles); $0.5/T_d$ (solid circles). Frame (d) is as in (c) with the same labels; but for $\widetilde{G}_-$. T and μ are in units of T_d and γ is unitless.

inert similar to an MI [65] and (2) that the weight of p-h excitations declines with increasing γ. This is shown in Fig. 8 frames (a) and (b), where $G(p = 0, \tau)$ decays at a faster rate with $|\tau|$ as γ is increased for any realization of the BCOL (we show here only two cases). In the limit when $\tau \to \pm\infty$, one can approximate $G(p = 0, \tau)$ by [15]

$$G(p = 0, \tau) \sim \begin{cases} e^{-E_P t} & ; \quad \tau \to +\infty \\ e^{+E_H t} & ; \quad \tau \to -\infty \end{cases} \tag{26}$$

where E_P and E_H are the single-particle and single-hole excitation energies, and $\tau = it$ is imaginary time. $G(p = 0, \tau)$ reveals that for larger γ and τ higher values of E_P and E_H are required to induce p-h excitations. The life-time of the p-h excitations $\sim \hbar/E_P$ or $\sim \hbar/E_H$, respectively, declines therefore with increasing γ as well. This demonstrates that because of the high repulsion the bosons become locked in their positions unable to move unless excited by a strong external perturbation. But even after they are excited, they are deexcited after a short time as they return to the OL. Moreover, $G(p = 0, \tau)$ is asymmetric about the origin $\tau = 0$, and particularly beyond the SG transition point γ_c, $G(p = 0, \tau)$ displays higher probability for hole excitations than particles.

One can obtain a weight for the particle (hole) excitations from an integration of the area under $G(p = 0, \tau)$ in the range $[0, \tau_{max}]$ ($[-\tau_{max}, 0]$), where $\tau_{max} = 250$ is the maximum value of τ. In fact, an integration from $-\tau_{max}$ to $+\tau_{max}$ would be approximately equivalent to the Fourier transform of $G(p = 0, \tau)$ at a frequency of excitation $\omega = 0$. We therefore consider for the present purpose

$$\widetilde{G}(p = 0, \omega) \sim \int_{-\tau_{max}}^{+\tau_{max}} G(p = 0, \tau) e^{-i\omega\tau} d\tau. \tag{27}$$

and separate it into two terms

$$\widetilde{G}(p = 0, \omega) = \widetilde{G}_+(p = 0, \omega) + \widetilde{G}_-(p = 0, \omega), \tag{28}$$

where

$$\begin{aligned} \widetilde{G}_+(p = 0, \omega) &\sim \int_0^{\tau_{max}} G(p = 0, \tau) e^{-i\omega\tau} d\tau, \\ \widetilde{G}_-(p = 0, \omega) &\sim \int_{-\tau_{max}}^0 G(p = 0, \tau) e^{-i\omega\tau} d\tau. \end{aligned} \tag{29}$$

One can then define $\widetilde{G}_+(p = 0, \omega = 0)$ and $\widetilde{G}_-(p = 0, \omega = 0)$ as the weights of particle and hole excitations, respectively. $\omega = 0$ is chosen because there is no excitation agent in our simulations.

Frames (c) and (d) display $\widetilde{G}_+(0, 0)$ and $\widetilde{G}_-(0, 0)$ as functions of γ, for $V_0 = 1.579/T_d$ and some values of V_1. Obviously, $\widetilde{G}_\pm$ decline with increasing γ and, moreover, both frames show an apparent change in the curvature of $\widetilde{G}_\pm$ close to the critical γ_c at which the SG transition occurs. Therefore, the change in the sign of $\partial^2 \widetilde{G}_\pm(0, 0)/\partial\gamma^2$ is a signal for the SG transition, and $\partial^2 \widetilde{G}_\pm(0, 0)/\partial\gamma^2 = 0$ near $\gamma = \gamma_c$.

TABLE II: Standard deviation of the BCOL δV [Eq.(2)] and Δ/J [cf. Eqs.(5) and (6)] for various realizations of the BCOL (1). From left to right the table lists the primary OL depth V_0, the secondary depth V_1, the standard deviation δV for $\alpha = 0.4$ and $\beta = 1.39$, δV for $\widetilde{\alpha} = 0.401248...$ and $\widetilde{\beta} = 1.389964...$, Δ/J for (α,β), and finally Δ/J for $(\widetilde{\alpha},\widetilde{\beta})$, respectively. V_0, V_1, δV are in units of (T_d), and Δ/J is unitless.

V_0 (T_d)	V_1 (T_d)	δV (α,β) (T_d)	δV $(\widetilde{\alpha},\widetilde{\beta})$ (T_d)	Δ/J (α,β)	Δ/J $(\widetilde{\alpha},\widetilde{\beta})$
1.579	0.1	0.5594	0.5595	0.2395	0.2380
	0.5	0.5856	0.5857	1.1977	1.1900
	0.7	0.6107	0.6108	1.6768	1.6600
6.316	1.0	2.2609	2.2613	16.712	16.6032
	3.0	2.4721	2.4726	50.138	49.8094

V. RATIONAL VS IRRATIONAL λ_1/λ_2

Whereas the ratio $\beta/\alpha = \lambda_1/\lambda_2$ is clearly rational for both pairs of $(\alpha,\beta) = (0.4, 1.0)$ and $(0.4, 1.39)$, it could be argued that had one used for example the irrational values $\widetilde{\alpha} = \sqrt{0.161} = 0.401248\cdots$ which is very close to 0.4, or $\widetilde{\beta} = \sqrt{1.9320} = 1.389964\cdots$ close to 1.39, the same results would be gotten as for $(0.4, 1.39)$. Within this context, Table II lists δV [Eq.(2)] and Δ/J [Eqs.(5) and (6)] for various realizations of the BCOL at $(\widetilde{\alpha},\widetilde{\beta})$ and the rational approximation (α,β). It can be seen that the results of δV and Δ/J for (α,β) differ only slightly from that for $(\widetilde{\alpha},\widetilde{\beta})$ by an order of magnitude $\lesssim 1\%$. In that sense, there should not be much difference in the results because of rational and irrational λ_1/λ_2.

VI. CONCLUSION

In summary then, the properties of bosons in a shallow 1D bichromatic optical lattice (BCOL), with a rational ratio λ_1/λ_2 of its wavelengths, have been examined by scanning the system along a range of the Lieb-Liniger parameter γ in the regime of the Sine-Gordon (SG) transition [5] at commensurate filling of the primary OL.

The chief result is that this transition in a primary OL of depth $V_0 \sim 1.5/T_d$ is robust against the perturbations by a secondary OL of depth $V_1 < V_0$. The critical interaction strength γ_c at which the transition occurs remains the same as for the periodic OL. The corresponding behavior of the superfluid fraction ρ_s/ρ vs γ reveals absolutely no response to changes in V_1; this is quite the same for other properties such as the correlation function $g_2(r)$ and the one-body density matrix $g_1(r)$. In contrast, changes in the latter observables arise with V_1 for larger values of $V_0 \sim 6/T_d$ at which the lattice-band structure of the primary OL begins to be influenced by the secondary OL.

However, for $V_0 \sim 1.5/T_d$ the properties are significantly affected by changes in γ. In this regard, $g_2(r)$ demonstrates an oscillatory structure whose amplitude rises with γ and V_0, manifestating an increase in the interplay between BCOL and interactions that yield the excitation of higher harmonics in the density operator. The origin of these oscillations lies chiefly in the primary OL. The latter changes are particularly significant beyond γ_c reaching deep into the SG regime signalling the presence of a non-inert Mott insulator in the form of a particle-hole gas of bosons. At very large γ beyond the critical γ_c, $g_2(0) \to 0$ signals fermionization and entrance to the Tonks-Girardeau regime. The fermionization process is aided by the primary OL and is unaffected by the secondary OL. Since $g_2(r)$ has been measured experimentally [17] over a broad range of the coupling strengths, our work should then motivate a future experimental measurement of $g_2(0)$ in a BCOL.

Although a division of $g_2(r)n_0^2$ and $g_1(r)n_0$ by the convoluted densities $\rho_c(r)$ and $\rho_{c,\frac{1}{2}}(r)$, respectively, yields qualitatively the same results as far as the sensitivity to changes in the BCOL is concerned, the response of $h_2(r) = g_2(r)n_0^2/\rho_c(r)$ to changes in V_0 and γ is in general significantly weakened. Hence, $g_2(r)$ is more adequate for obtaining stronger signals of changes. The $g_2(r)$ displays oscillations arising from oscillations in the spatial density that account for the same behavior in the density-density correlations.

The MGF $G(p = 0, \tau)$ displays a declining weight for the particle-hole excitations with rising γ attributed to an increased localization of the bosons. Moreover, it has been found that the system favors hole excitations at strong interactions leading us to conclude that deep in the SG regime holes play a chief role in the response of $g_1(r)$ and $g_2(r)$ to γ. In addition, a change in the curvature of the Fourier transform of the MGF $G(p = 0, \omega = 0)$ as a function of γ for either particles or holes, is a signal for the SG transition.

It has been particularly argued, that there shouldn't be much difference between the results obtained by using an irrational λ_1/λ_2 and a rational approximation to the same λ_1/λ_2 basing on the fact that the disorder strength of a BCOL changes only by small percentages if one uses a rational approximation to, instead of an irrational, λ_1/λ_2.

Finally, it must be emphasized that the WA applied here has been tested for accuracy. By making comparions with previous results, it has been shown that the WA code works correctly and is therefore reliable. For example, our results for $g_1(r)$ are in very good agreement with those computed by Astrakharchik and Giorgini [57]. Moreover, the superfluid behavior with temperature matches exactly an analytical calculation from Ref.[61]. Most importantly, the WA code was able to reproduce the SG transition observed earlier by Haller *et al.* [5]. The current results are also in line with Edwards *et al.* [66] who demonstrated that the effects of weak perturbations to a primary 1D OL disappear as interactions get stronger and we *are* in the strongly interacting regime. During the preparation of this paper, we learnt of an in-

vestigation bearing similarities to ours by Boéris *et al.* [16] where, among other issues, the WA has been applied to reproduce the SG transition, except that they only use a periodic OL with a different procedure than ours here.

Acknowledgments

Interesting and enlightning discussions with Sebastiano Pilati (ICTP, Trieste, Italy) are gratefully acknowledged and particulary for suggesting the topic on the Sine-Gordon transition. Additional thanks go to Nikolay Prokofiev (UMASS, Amherst, USA) for interesting discussions and for providing the worm algorithm code. The author wishes to thank the Abdus-Salam International Center for Theoretical Physics (ICTP) in Trieste, Italy, and the Max Planck Institute for Physics of Complex Systems (MPIPKS) in Dresden Germany, both for providing him access to their excellent computational cluster and for a hospitable stay during scientific visits in which this work was undertaken. We are grateful to G. Astrakharchik for providing us with their data displayed in Fig. 1. We thank William J. Mullin (UMASS, Amherst, USA) for a critical reading of the manuscript.This work has been carried out during the sabbatical leave granted to the author Asaad R. Sakhel from Al-Balqa Applied University (BAU) during academic year 2014/2015.

Appendix A: Worm Algorithm

Specifically, a WA code is applied which has been written by Nikolay Prokofev [55] originally for the simulation of 1D soft-core bosons without any trapping potential. A 3D version of this code, although for ^{4}He on graphite, has been described earlier [53]. WA is a path-integral Monte Carlo technique whose configurational space is extended to include what one calls "worms". In this method, particles are described by Feynman's path-integral formulation as closed trajectories in space-time (diagonal configurations). Each trajectory is a closed chain of "beads" and each "bead" is a pair of positions of the same particle separated by a time τ along the imaginary-time axis in space-time. In a closed trajectory, the initial and final positions of the path are the same along the space axis. The method considers imaginary "time" as inverse temperature [67], i.e., $it/\hbar \leftrightarrow 1/(k_BT)$, where $\hbar$ is Planck's constant, k_B Boltzmann's constant, and T the temperature. The configuration of the system is updated by adding or removing open trajectories in space-time called "worms" (off-diagonal configurations) which are paths in space-time whose initial and final positions along the space axis are not the same. Therefore, the configuration of the system is divided into two sectors: the $Z-$sector containing all the closed trajectories and the $G-$sector containing one open trajectory, or worm. The code is designed to perform various updates on these worms via certain acceptance and rejection probabilities that are carefully weighted functions of, and including, the factors $\exp[-(\mathbf{r}_\ell - \mathbf{r}_{\ell-1})^2/(4\lambda\tau)]$ and $\exp[-\tau V(\mathbf{r}_\ell)]$. Here $\lambda = \hbar^2/(2m)$ with m the mass of a boson, $\tau \to 1/(Mk_BT)$ is the imaginary time step with M the total number of beads constituting the particle's trajectory along the imaginary time axis, $\mathbf{r}_\ell$ is the position of the ℓ^{th} bead along the space axis, and $V(\mathbf{r}_\ell)$ is the potential energy of bead ℓ. The above factors included in a worm-update probability are integrated along the time axis over the length of the worm being updated. The beginning and end of the worm are termed MASHA and IRA, respectively, where MASHA precedes IRA along the imaginary time axis. There are various types of updates: (1) INSERT or REMOVE in which a worm is created and added to, or annihilated from, the configuration, respectively; (2) MOVE FORWARD or MOVE BACKWARD that change the length of the worm in space-time along the imaginary time axis; (3) RECONNECT in which a worm is connected to a closed trajectory after opening it resulting in an exchange of particles (permutation); (4) CUT or GLUE where a closed trajectory is cut open by removing, or an open trajectory is closed by adding, a short chain of beads, respectively. All these updates are described in more detail by the inventors of the technique [53].

Appendix B: Pair correlation function for inhomogeneous 1D Bose gases

Fig. 9 is as in Fig. 4; but for $h_2(r)$ given by Eq.(14). In frame (A) for low V_0, the amplitude of the spatial oscillations in $h_2(r)$ is substantially reduced compared to the corresponding $g_2(r)$. Although the $h_2(r)-$oscillations do not vanish completely, their amplitude does not change with V_1 that is the same for $g_2(r)$ in Fig. 4(A). Indeed, the $g_2(r)-$oscillations are caused by the oscillations in the convoluted density $\rho_c(r)$ [Eq.(13)], and a division of $g_2(r)n_0^2$ by $\rho_c(r)$ [to get $h_2(r)$] almost flattens $h_2(r)$ at larger r so that it oscillates close to 1. Any changes in the structure of $h_2(r)$ with V_1 are not detected. There is a weak role of the band structure of the BCOL and its disorder at low V_0 which is consistent with Fig. 5.

As one increases V_0 in Fig. 9(B), the amplitude of oscillations in $h_2(r)$ rises similarly to $g_2(r)$. This time the normalization by $\rho_c(r)$ does not yield a significant suppression of the oscillations as it occurs in frame (A). Therefore, at larger V_0 the origin of these oscillations may not be anymore chiefly the oscillations in the spatial density; rather they largely arise from an increased effect of the band structure of the BCOL and the disorder; the latter is again consistent with the increase of disorder with V_0 in Fig. 5. Qualitatively nevertheless, Fig. 9 shows the same effects as Fig. 4, that is to say, that by either $g_2(r)$ or $h_2(r)$, one reaches qualitatively the same conclusions about the effect of V_1 on the strength of the correlations, namely that there is none at low V_0.

Fig. 10 is the same as Fig. 6; but for $h_2(r)$. Here, the

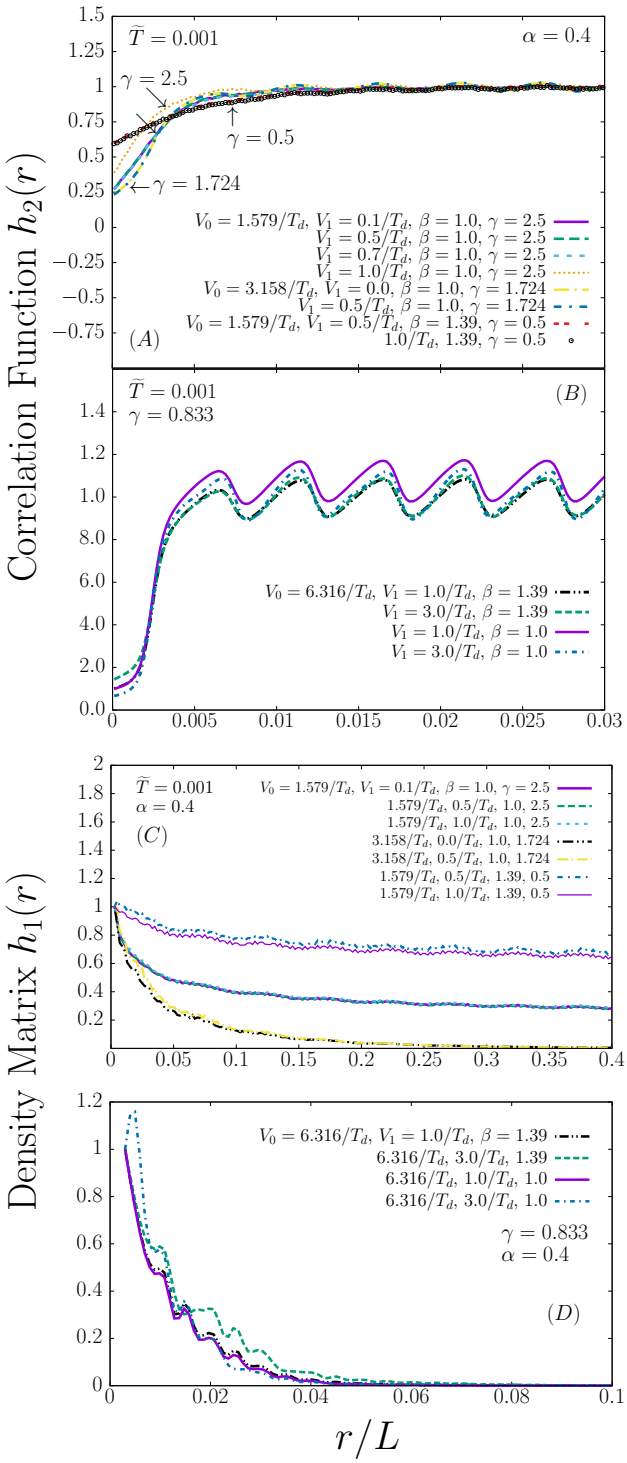
Correlation Function $h_2(r)$
Density Matrix $h_1(r)$
r/L
$\widetilde{T} = 0.001$
$\alpha = 0.4$
$\gamma = 2.5$
$\gamma = 0.5$
$\leftarrow \gamma = 1.724$
$V_0 = 1.579/T_d$, $V_1 = 0.1/T_d$, $\beta = 1.0$, $\gamma = 2.5$
$V_1 = 0.5/T_d$, $\beta = 1.0$, $\gamma = 2.5$
$V_1 = 0.7/T_d$, $\beta = 1.0$, $\gamma = 2.5$
$V_1 = 1.0/T_d$, $\beta = 1.0$, $\gamma = 2.5$
$V_0 = 3.158/T_d$, $V_1 = 0.0$, $\beta = 1.0$, $\gamma = 1.724$
$V_1 = 0.5/T_d$, $\beta = 1.0$, $\gamma = 1.724$
$V_0 = 1.579/T_d$, $V_1 = 0.5/T_d$, $\beta = 1.39$, $\gamma = 0.5$
$1.0/T_d$, 1.39, $\gamma = 0.5$
(A)
$\widetilde{T} = 0.001$
$\gamma = 0.833$
(B)
$V_0 = 6.316/T_d$, $V_1 = 1.0/T_d$, $\beta = 1.39$
$V_1 = 3.0/T_d$, $\beta = 1.39$
$V_1 = 1.0/T_d$, $\beta = 1.0$
$V_1 = 3.0/T_d$, $\beta = 1.0$
$\widetilde{T} = 0.001$
$\alpha = 0.4$
(C)
$V_0 = 1.579/T_d$, $V_1 = 0.1/T_d$, $\beta = 1.0$, $\gamma = 2.5$
$1.579/T_d$, $0.5/T_d$, 1.0, 2.5
$1.579/T_d$, $1.0/T_d$, 1.0, 2.5
$3.158/T_d$, $0.0/T_d$, 1.0, 1.724
$3.158/T_d$, $0.5/T_d$, 1.0, 1.724
$1.579/T_d$, $0.5/T_d$, 1.39, 0.5
$1.579/T_d$, $1.0/T_d$, 1.39, 0.5
$V_0 = 6.316/T_d$, $V_1 = 1.0/T_d$, $\beta = 1.39$
$6.316/T_d$, $3.0/T_d$, 1.39
$6.316/T_d$, $1.0/T_d$, 1.0
$6.316/T_d$, $3.0/T_d$, 1.0
$\gamma = 0.833$
$\alpha = 0.4$
(D)

FIG. 9: (Color online) As in Fig. 6; but for $h_2(r)$. Upper frame (A): at $\gamma = 2.5$ and $V_0 = 1.579/T_d$ the figure displays the results for: $V_1 = 0.1/T_d$, $\beta = 1.0$ (thick solid line); 0.5, 1.0 (thick-dashed line); 0.7, 1.0 (short-dashed line); 1.0, 1.0 (fine-dotted line). Then at $\gamma = 1.724$ and $V_0 = 3.158/T_d$ the results for: 0.0, 1.0 (long-dashed dotted line); 0.5, 1.0 (short-dashed dotted line). At $\gamma = 0.5$ and $V_0 = 1.579/T_d$ again the results are shown for: $V_1 = 0.5/T_d$, $\beta = 1.39$ (double-dotted dotted line); 1.0, 1.39 (open circles). Upper frame (B) is for $V_0 = 6.316/T_d$, $\gamma = 0.833$, and: $V_1 = 1.0/T_d$, $\beta = 1.39$ (long-dashed double-dotted line); $3.0/T_d$, 1.39 (thick-dashed line); $1.0/T_d$, 1.0 (thin-dashed line); $3.0/T_d$, 1.0 (dashed-dotted line). Lower frame (C) is for the same system in (A); but for $h_1(r)$ with $V_0 = 1.579/T_d$ and: $V_1 = 0.1/T_d$, $\beta = 1.0$, $\gamma = 2.5$ (thick solid line); $0.5/T_d$, 1.0, 2.5 (thick-dashed line); $1.0/T_d$, 1.0, 2.5 (thin-dashed line). Then one has for $V_0 = 3.158/T_d$: $0.0/T_d$, 1.0, 1.724 (long-dashed double-dotted line); $0.5/T_d$, 1.0, 1.724 (dashed-dotted line). Next one has for $V_0 = 1.579/T_d$: $0.5/T_d$, 1.39, 0.5 (short-dashed dotted line); $1.0/T_d$, 1.39, 0.5 (thin solid line). Finally frame (D) is for the same system in (B); but for $h_1(r)$: dashed double-dotted line: $V_1 = 1.0/T_d$, $\beta = 1.39$; dashed line: $3.0/T_d$, 1.0; thick solid line: $1.0/T_d$, 1.0; dashed-dotted line: $3.0/T_d$, 1.0.

effect of interactions γ at $r > 0.00025$ is substantially weakened in by the division of $g_2(r)n_0^2$ by $\rho_c(r)$, but remains quite pronounced towards $r \to 0$. The effect of γ at larger r cannot therefore be significantly detected by $h_2(r)$ because the effect of interactions is absorbed by the normalization process. At $r = 0$, $h_2(r)$ displays a reduction with γ similar to Fig. 6 and shows the same decline as in Fig. 7 (see Sec.D below).

Appendix C: One-body density matrix for inhomogeneous 1D Bose gases

The SA-OBDM $h_1(r)$ [Eq.(16)] in frames (C) and (D) of Fig. 9 displays qualitatively the same behavior as the corresponding $g_1(r)$, except for small oscillations that are a result of normalizing by $\rho_{c,\frac{1}{2}}(r)$. In fact, at larger V_0, there is really not much difference in the qualitative

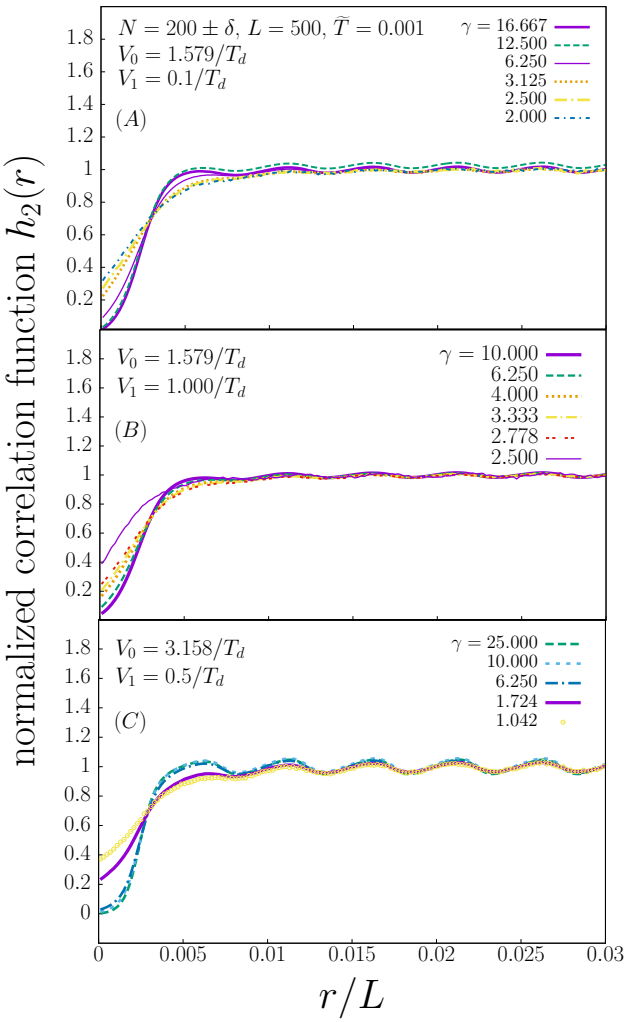

FIG. 10: As in Fig. 6; but for $h_2(r)$. Frame (A): $V_0 = 1.579/T_d$, $V_1 = 0.1/T_d$ and: $\gamma = 16.667$ (thick-solid line); 12.500 (dashed line); 6.250 (thin solid line); 3.125 (fine-dotted line); 2.500 (long-dashed dotted line); 2.000 (short-dashed dotted line). Frame (B) is for $V_0 = 1.579/T_d$, $V_1 = 1.000/T_d$ and: $\gamma = 10.000$ (solid line); 6.250 (dashed line); 4.000 (fine-dotted line); 3.333 (dashed-dotted line); 2.778 (double-dotted line); 2.500 (thin solid line). Frame (C): $V_0 = 3.158$, $V_1 = 0.5/T_d$, and: $\gamma = 25.000$ (thick-dashed line); 10.000 (thin-dashed line); 6.250 (dashed-dotted line); 1.724 (thick-solid line); 1.042 (circles).

structure of $h_1(r)$ and $g_1(r)$ in frames (D) of Figs. 9 and 4, respectively −both of them display small oscillations. Therefore for larger V_0, $h_1(r)$ and $g_1(r)$ can both be applied on the same footage to draw conclusions about the superfluid depletion and role of the BCOL.

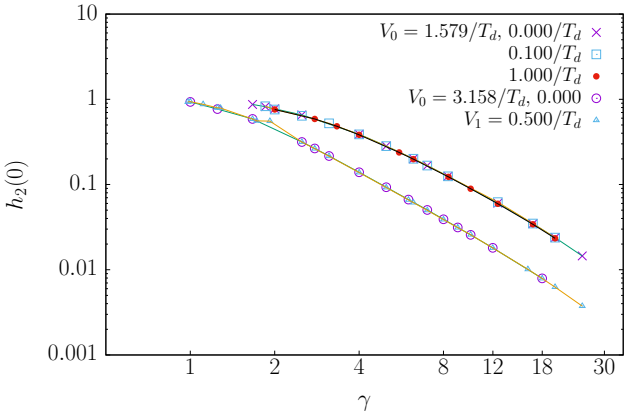

FIG. 11: As in Fig. 7; but for $h_2(0)$ with $V_0 = 1.579/T_d$ and: $V_1 = 0$ (times); $0.1/T_d$ (open square); $1.0/T_d$ (solid circles). Next data is for $V_0 = 3.158$ and: $V_1 = 0$ (open circles) and $0.5/T_d$ (open triangles).

Appendix D: Local correlation function for inhomogeneous 1D Bose gases

The SAPCF at $r = 0$, i.e. $h_2(0)$, displays in Fig. 11 a drop with increasing γ and shows almost the same behavior as $g_2(0)$ in Fig. 7. Again, changes in V_1 for the same V_0 have no effect on $h_2(0)$.

[1] P. Sengupta, M. Rigol, G. G. Batrouni, P. J. H. Denteneer, and R. T. Scalettar, Phys. Rev. Lett. **95**, 220402 (2005).

[2] Xia-Ji Liu, Peter D. Drummond, and Hui Hu, Phys. Rev. Lett. **94**, 136406 (2005).

[3] S. R. Clark and D. Jaksch, Phys. Rev. A **70**, 043612 (2004).

[4] S. Ramanan, T. Mishra, M. S. Luthra, R. V. Pai, and B. P. Das, Phys. Rev. A **79**, 013625 (2009).

[5] Elmar Haller, Russel Hart, Manfred J. Mark, Johann G. Danzl, Lukas Reichsöllner, Mattias Gustavsson, Marcello Dalmonte, Guido Pupillo, and Hanns-Christoph Nägerl, Nature **466**, 597 (2010).

[6] H. P. Büchler, G. Blatter, and W. Zwerger, Phys. Rev. Lett. **90**, 130401 (2003).

[7] T. Giamarchi, *Quantum Physics in One Dimension* (Oxford Univ. Press, 2003), 1st ed.

[8] Ming-Xia Huo and Dimitris G. Angelakis, Phys. Rev. A **85**, 023821 (2012).

[9] E. H. Lieb and W. Liniger, Phys. Rev. **130**, 1605 (1963).

[10] L. Guidoni, C. Triché, P. Verkerk, and G. Grynberg, Phys. Rev. Lett. **79**, 3363 (1997).

[11] Nicolas Nessi and Anibal Iucci, Phys. Rev. A **84**, 063614 (2011).

[12] M. C. Gordillo, C. Carbonell-Coronado, and F. De Soto, Phys. Rev. A **91**, 043618 (2015).

[13] Mohammad Hafezi, Darrick E. Chang, Vladimir Gritsev, Eugene Demler, and Mikhail D. Lukin, Phys. Rev. A **85**, 013822 (2012).

[14] C. J. Pethick and H. Smith, *Bose-Einstein Condensation in Dilute Gases* (Cambridge University Press, Cambridge UK, 2002), 1st ed.

[15] Maciej Lewenstein, Anna Sanpera, and Verónica Ahufinger, *Ultracold Atoms in Optical Lattices: Simulating Quantum Many-Body Systems* (Oxford University Press, United Kingdom, 2012).

[16] G. Boéris, L. Gori, M. D. Hoogerland, A. Kumar, E. Lucioni, L. Tanzi, M. Inguscio, T. Giamarchi, C. DErrico, G. Carleo, G. Modugno, and L. Sanchez-Palencia, Phys. Rev. A **93**, 011601(R) (2016).

[17] Toshiya Kinoshita, Trevor Wenger, and David S. Weiss, Phys. Rev. Lett. **95**, 190406 (2005).

[18] B. Deissler, E. Lucioni, M. Modugno, G. Roati, L. Tanzi, M. Zaccanti, M. Inguscio, and G. Modugno, New J. Phys. **13**, 023020 (2011).

[19] G. Roux, T. Barthel, I. P. McCulloch, C. Kollath, U. Schollwöck, and T. Giamarchi, Phys. Rev. A **78**, 023628 (2008).

[20] Tommaso Roscilde, Phys. Rev. A **77**, 063605 (2008).

[21] M. Larcher, M. Modugno, and F. Dalfovo, Phys. Rev. A **83**, 013624 (2011).

[22] Michele Modugno, New J. Phys. **11**, 033023 (2009).

[23] R. Roth and K. Burnett, Phys. Rev. A **67**, 031602(R) (2003).

[24] S. Pilati, S. Giorgini, M. Modugno, and N. Prokof'ev, New J. Phys. **12**, 073003 (2010).

[25] I. L. Aleiner, B. L. Altshuler, and G. V. Shlyapnikov, Nature Phys. **6**, 900 (2010).

[26] P. Lugan, A. Aspect, L. Sanchez-Palencia, D. Delande, B. Grémaud, C. A. Müller, and C. Miniatura, Phys. Rev. A **80**, 023605 (2009).

[27] M. White, M. Pasienski, D. McKay, S. Q. Zhou, D. Ceperley, and B. DeMarco, Phys. Rev. Lett. **102**, 055301 (2009).

[28] L. Fallani, J. E. Lye, V. Guarrera, C. Fort, and M. Inguscio, Phys. Rev. Lett. **98**, 130404 (2007).

[29] B. Deissler, M. Zaccanti, G. Roati, C. DÉrrico, M. Fattori, M. Modugno, G. Modugno, and M. Inguscio, Nature Phys. **6**, 354 (2010).

[30] Giacomo Roati, Chiara DÉrrico, Leonardo Fallani, Marco Fattori, Chiara Fort, Matteo Zaccanti, Giovanni Modugno, Michele Modugno, and Massimo Inguscio, Nature **453**, 895 (2008).

[31] Juliette Billy, Vincent Josse, Zhanchun Zuo, Alain Bernard, Ben Hambrecht, Pierre Lugan, David Clément, Laurent Sanchez-Palencia, Philippe Bouyer, and Alain Aspect, Nature Phys. Lett. **453**, 891 (2008).

[32] Yong P. Chen, J. Hitchcock, D. Dries, M. Junker, C. Welford, and R. G. Hulet, Phys. Rev. A **77**, 033632 (2008).

[33] Matthew P. A. Fisher, Peter B. Weichman, G. Grinstein, and Daniel S. Fisher, Phys. Rev. B **40**, 546 (1989).

[34] Jacques Bossy, Jonathan V. Pearce, Helmut Schober, and Henry R. Glyde, Phys. Rev. B **78**, 224507 (2008).

[35] S. Palpacelli and S. Succi, Phys. Rev. E **77**, 066708 (2008).

[36] D. Clément, A. F. Varón, J. A. Retter, L. Sanchez-Palencia, A. Aspect, and P. Bouyer, New J. Phys. **8**, 165 (2006).

[37] X. Deng, R. Citro, E. Orignac, A. Minguzzi, and L. Santos, Phys. Rev. B **87**, 195101 (2013).

[38] L. Pollet, N. V. Prokof'ev, and B. V. Svistunov, Phys. Rev. B **87**, 144203 (2013).

[39] Z. Ristivojevic, A. Petković, P. Le Doussal, and T. Giamarchi, Phys. Rev. Lett. **109**, 026402 (2012).

[40] Shankar Iyer, David Pekker, and Gil Rafael, Phys. Rev. B **88**, 220501(R) (2013).

[41] D. M. Basko and F. W. J. Hekking, Phys. Rev. B **88**, 094507 (2013).

[42] T. Schulte, S. Drenkelforth, J. Kruse, W. Ertmer, J. Arlt, K. Sacha, J. Zakrzewski, and M. Lewenstein, Phys. Rev. Lett. **95**, 170411 (2005).

[43] T. Paul, P. Schlagheck, P. Leboeuf, and N. Pavloff, Phys. Rev. Lett. **98**, 210602 (2007).

[44] L. Sanchez-Palencia, D. Clément, P. Lugan, P. Bouyer, G. V. Shlyapnikov, and A. Aspect, Phys. Rev. Lett. **98**, 210401 (2007).

[45] P. Lugan, D. Clément, P. Bouyer, A. Aspect, and L. Sanchez-Palencia, Phys. Rev. Lett. **99**, 180402 (2007).

[46] T. Paul, M. Albert, P. Schlagheck, P. Leboeuf, and N. Pavloff, Phys. Rev. A **80**, 033615 (2009).

[47] J. Radić, V. Bačić, D. Jukić, M. Segev, and H. Buljan, Phys. Rev. A **81**, 063639 (2010).

[48] J. C. C. Cestari, A. Foerster, and M. A. Gusmão, Phys. Rev. A **82**, 063634 (2010).

[49] S. Iyer, D. Pekker, and G. Rafael, Phys. Rev. B **85**, 094202 (2012).

[50] C. Aulbach, A. Wobst, G. L. Ingold, P. Hänggi and I. Varga, New J. Phys. **6**, 70 (2004).

[51] D. J. Boers, B. Goedeke, D. Hinrichs and M. Holthaus, Phys. Rev. A **75**, 063404 (2007).

[52] Xiaolong Deng and Luis Santos, Phys. Rev. A **89**, 033632 (2014).

[53] M. Boninsegni, N. V. Prokof'ev, and B. V. Svistunov, Phys. Rev. E **74**, 036701 (2006).

[54] A. G. Sykes, D. M. Gangardt, M. J. Davis, K. Viering, M. G. Raizen, and K.V. Kheruntsyan, Phys. Rev. Lett. **100**, 160406 (2008).

[55] Nikolay Prokofev, UMASS Amherst, Private Communication.

[56] R. P. Feynman, *Statistical Mechanics* (Westview Press, Advanced Book Program, Boulder, Colorado, 1998).

[57] G. E. Astrakharchik, J. Boronat, J. Casulleras, and S. Giorgini, Phys. Rev. Lett. **95**, 190407 (2005).

[58] see Eq.(13.37) on page 349 in Ref.[14].

[59] The second-order correlation function for atoms in an OL is given by Lewenstein *et al.* [15] on page 419 and is effectively the same as ours:

$$g^{(2)}(\vec{\mathbf{d}}) = \frac{\int d\vec{\mathbf{r}} \langle \hat{n}(\vec{\mathbf{r}} + \vec{\mathbf{d}}/2)\hat{n}(\vec{\mathbf{r}} - \vec{\mathbf{d}}/2)\rangle}{\int d\mathbf{r} \langle \hat{n}(\vec{\mathbf{r}} + \vec{\mathbf{d}}/2)\rangle \langle \hat{n}(\vec{\mathbf{r}} - \vec{\mathbf{d}}/2)\rangle} - 1,$$

where $\vec{\mathbf{d}} = \vec{\mathbf{r}} - \vec{\mathbf{r}'}$ is the distance between two particles situated at $\vec{\mathbf{r}}$ and $\vec{\mathbf{r}'}$, and $\hat{n}(r)$ is the density operator.

[60] M. Naraschewski and R. J. Glauber, Phys. Rev. A **59**, 4595 (1999).

[61] Adrian Del Maestro and Ian Affleck, Phys. Rev. B **82**, 060515(R) (2010).
[62] Grigory E. Astrakharchik, Konstantin V. Krutitsky, Maciej Lewenstein, and Ferran Mazzanti, *One-dimensional Bose gas in optical lattices of arbitrary strength*, cond-mat/1509.01424.
[63] Alexander Yu. Cherny and Joachim Brand, Phys. Rev. A **79**, 043607 (2009).
[64] K. V. Kheruntsyan, D. M. Gangardt, P. D. Drummond, and G. V. Shlyapnikov, Phys. Rev. Lett. **91**, 040403 (2003).
[65] Stefan S. Natu and Erich J. Mueller, Phys. Rev. A **87**, 063616 (2013).
[66] E. E. Edwards, M. Beeler, Tao Hong, and S. L. Rolston, Phys. Rev. Lett. **101**, 260402 (2008).
[67] G. D. Mahan, *Many-Particle Physics* (Plenum Press, New York, 1990).